J. Fluid Mech. (2009), *vol.* 629, *pp.* 195–219.
doi:10.1017/S0022112009006533 Printed in the United Kingdom

Breakup of surfactant-laden jets above the critical micelle concentration

R. V. CRASTER[1], O. K. MATAR[2]† AND D. T. PAPAGEORGIOU[2,3]

[1]Department of Mathematical and Statistical Sciences, University of Alberta, Edmonton T6G 2G1, Canada

[2]Department of Chemical Engineering, Imperial College London, South Kensington Campus, London SW7 2AZ, UK

[3]Department of Mathematics, Imperial College London, South Kensington Campus, London SW7 2AZ, UK

(Received 11 November 2008 and in revised form 9 February 2009)

The breakup of viscous liquid jets that contain surfactant, that is potentially above the critical micelle concentration (CMC) is considered here within the long-wave approximation. The soluble surfactant is assumed to be present in three phases: as an interfacial species, bulk monomers and micelles. A model is developed for the interaction between these phases and the surface tension which obeys a nonlinear equation of state. The effects of the equation of state and the reservoir of surfactant created by micelles on breakup are investigated. The long-wave approximation naturally leads to a system of coupled one-dimensional equations that are solved numerically. It is demonstrated that jet breakup and satellite formation are critically affected by the presence of high surfactant concentrations above the CMC. This manifests itself by the formation of unusually large satellites. We present extensive numerical evidence that the mechanism for this phenomenon centres on the interplay between Marangoni stresses and the nonlinear surfactant equation of state; the latter exhibits a plateau at high interfacial concentrations.

1. Introduction

The breakup of jets and threads has received considerable attention in the literature since the seminal theoretical work of Rayleigh (1878), and the subsequent analyses of Tomotika (1935) and Chandrasekhar (1961); this is due to the obvious relevance of jet breakup to fluid mixing, ink-jet printing and microfluidic applications (Anna, Bontoux & Stone 2003; Link *et al.* 2004; Wang, Mohebi & Evans 2005). The large number of papers that have appeared since these studies have been summarized in reviews by Denn (1980), Eggers (1997), Lin & Reitz (1998) and Eggers & Villermaux (2008). Research in this area has included linear temporal (Tomotika 1935; Chandrasekhar 1961; Rayleigh 1878) and spatial (Keller, Rubinow & Tu 1973; Leib & Goldstein 1986*a*, *b*; Chauhan *et al.* 2003) analyses; in the latter case, the growth of disturbances in the axial direction is examined. Indeed, as shown in Chauhan *et al.* (2003), spatial instabilities tend to dominate over temporal ones provided a threshold Weber number is exceeded.

† Email address for correspondence: o.matar@imperial.ac.uk

Given the long and thin nature of a jet of fluid there has been considerable interest in developing one-dimensional models to study the nonlinear stability of jets, starting with the work of Lee (1974) and continuing with the studies of Eggers (1993, 1995, 1997), Schulkes (1993), Eggers & Dupont (1994) and Papageorgiou (1995*a*, *b*). The theory for Stokes flow by Papageorgiou and that for the viscous-inertial regime by Eggers *et al.*, which are based on the construction of local similarity solutions as breakup is approached, have been verified experimentally (McKinely & Tripathi 2000; Rothert, Richter & Rehberg 2003). Other one-dimensional studies include the work of Brenner, Shi & Nagel (1994), Shi, Brenner & Nagel (1994), Notz, Chen & Basaran (2001) and Chen, Notz & Basaran (2002) and these have been complemented by direct numerical simulations of the two-dimensional Navier–Stokes equations (Wilkes, Phillips & Basaran 1999; Ambravaneswarn, Wilkes & Basaran 2002) as well as experimental work (Zhang, Harris & Basaran 1994; Zhang & Basaran 1995). Ambravaneswaran *et al.* (2002) have also found good agreement between the predictions of the one-dimensional models with those of numerical solutions of the Navier–Stokes equations.

Although surfactant effects are undoubtedly important there has been considerably less work in this area, and the majority is based upon an assumption that the surfactant is insoluble in the bulk. The effect of insoluble surfactants on the breakup of jets and threads (Hansen, Peters & Meijer 1999; Kwak & Pozrikidis 2001; Craster, Matar & Papageorgiou 2002; Timmermans & Lister 2002), the stability and breakup of liquid bridges (Ambravaneswaran & Basaran 1999; Liao, Franses & Basaran 2006), the deformation of droplets under extensional (Eggleton & Stebe 1998; Eggleton, Pawar & Stebe 1999) and shear (Bazhlekov, Anderson & Meijer 2006) flow, the detachment of viscous drops (Jin, Gupta & Stebe 2006) and the breakup of stretched bubbles in viscous liquids (Hameed *et al.* 2008) has been examined in detail. These studies have demonstrated the profound effect that surfactants can have on the dynamics of necking and satellite drop formation: when the thread is surrounded by another viscous fluid, the presence of surfactants retards the thinning processes and leads to the development of secondary necks in the vicinity of a satellite drop (Kwak & Pozrikidis 2001; Timmermans & Lister 2002); surfactants also decrease the size of satellite drops when the thread is surrounded by vacuum as noted by Craster *et al.* (2002). The work of Craster *et al.* (2002), which is based on the derivation of evolution equations for the interfacial location, insoluble surfactant concentration and the axial velocity component using long-wave theory, demonstrated that despite the presence of surfactant, the behaviour near pinching remains governed by the similarity solution of Eggers (1993). More recently, the work of McGough & Basaran (2006) has demonstrated the possibility of repeated filament formation during the breakup of threads covered with an insoluble surfactant even in the absence of noise; the presence of noise is a necessity in the case of surfactant-free threads (Shi *et al.* 1994).

The effect of surfactant solubility on the stability of jets has also been studied. Jin, Gupta & Stebe (2006) showed numerically that surfactant accumulation at the location of maximal interfacial contraction reduces the local surface tension and retards thinning; this is governed by the adsorption and desorption kinetics at the interface. Liao *et al.* (2004) demonstrated experimentally that breakup of a liquid bridge becomes increasingly asymmetric with increasing soluble surfactant concentration due to the lowering of the local surface tension in relation to gravity. The limiting lengths of liquid bridges was also found to increase with soluble surfactant concentration, particularly above the critical micelle concentration (CMC). Satellite

formation was noticeably absent provided bridge-stretching time scales exceeded those associated with surfactant adsorption from the bulk onto the interface.

The behaviour of micellar surfactant solutions is quite distinct from that of monomeric solutions and models are developed in this paper to incorporate and study such differences. At equilibrium, the state of the surfactant in solution changes at the CMC. For bulk concentrations below CMC, $C < \mathrm{CMC}$, where C is the bulk concentration, surfactants are present as monomers in solution which do not aggregate but exist as single molecules. As the bulk concentration increases above the CMC (i.e. $C > \mathrm{CMC}$), micelles form; these are fluid-like aggregates with an aggregation number n which is typically about 50–100. The aggregates form with their hydrophobic tails oriented towards the centre of the micelle and their hydrophilic heads oriented towards the fluid solvent. For bulk concentrations above the CMC the concentration of monomers attains the uniform value at the CMC and monomers coexist (at constant chemical potential) with micelles which are made up of the remaining surfactant molecules in solution.

When an interface is present there is a strong change in the surface concentration of surfactant Γ as the bulk concentration C increases. For bulk concentrations $C <$ CMC, the addition of surfactants to the solution increases the bulk chemical potential μ (not to be confused with viscosity later used in the paper), which in turn increases the interface chemical potential denoted by μ_s. A relationship between C and Γ, the Langmuir adsorption isotherm, can be found by equating μ and μ_s and assuming an ideal bulk solution and no interactions of adsorbed species on the interface. Defining the maximum (unattainable) packing interfacial concentration as Γ_∞ and considering sufficiently dilute bulk solutions, we have the following expressions for the chemical potentials: $\mu = \mu_0(T) + R_g T \ln C$, and $\mu_s = \mu_{s0}(T) + R_g T \ln((\Gamma/\Gamma_\infty)/(1 - \Gamma/\Gamma_\infty))$, where (μ_0, μ_{s0}) represent reference chemical potentials, T is the temperature and R_g is the universal gas constant. Equating these leads to the Langmuir equilibrium relationship $C = \chi(\Gamma/\Gamma_\infty)/(1 - \Gamma/\Gamma_\infty)$ with $\chi = \exp((\mu_{s0}(T) - \mu_0(T))/R_g T)$, which is equivalent to the equilibrium version of the flux relationship given later in (2.8*a*). On the other hand if the bulk concentration is above the CMC ($C > \mathrm{CMC}$), the chemical potentials of the bulk and interface are constant; this in turn implies that as surfactant is added to the system the surface concentration saturates to a constant value Γ_c.

The variations in surface surfactant concentration affect the surface tension. As described above for $C <$ CMC, addition of surfactant to the bulk increases Γ and this implies a decrease in the surface tension γ due to the isothermal Gibbs adsorption equation, $\mathrm{d}\gamma = -\Gamma\,\mathrm{d}\mu = -\Gamma\,\mathrm{d}\mu_s$. At equilibrium as C increases above the CMC, however, the surface concentration remains constant at Γ_c and the surface tension also remains constant at a value $\gamma(\Gamma_c)$. This implies that at equilibrium and for $C > CMC$, there is a decoupling between the values of the surface tension and the addition of surfactant in the bulk.

The phenomena described above are valid at equilibrium when the chemical potentials of the bulk and interface are equal. If kinetic barriers exist, however, then inequalities between the chemical potentials arise. In the present work we incorporate the effects of kinetic barriers into our models and evaluate numerically their impact on the dynamics of liquid jets. In what follows we provide a brief overview of the general phenomena that are possible in such cases but emphasize that simulations are typically required to quantify the physics. Inequalities between the chemical potentials of the bulk and interface can occur in a system that develops dynamically if the time scales required to equilibrate bulk and surface chemical

potentials are longer than those imposed by the underlying flow dynamics. There are two mechanisms by which equilibrium can be disrupted by the presence of kinetic barriers. First, if the desorption kinetics is hindered then this leads to a difference between bulk and surface chemical potentials. Several examples can be constructed: (i) If we are at equilibrium with a bulk concentration below CMC, and the solution in the bulk is suddenly diluted, then in the presence of kinetic barriers that hinder desorption, the surface concentration Γ will be out of equilibrium with the suddenly reduced bulk concentration. (ii) If we are at equilibrium with a bulk concentration below CMC and a surface element is suddenly contracted, then if desorption into the bulk is hindered we end up with surface concentrations above the equilibrium value. (iii) If initially we are at equilibrium with a bulk concentration above CMC $C >$ CMC and corresponding surface concentration Γ_c, and a surface element is suddenly contracted while desorption into the bulk is hindered, then we can obtain values of $\Gamma > \Gamma_c$ which in turn imply values of the surface tension below $\gamma(\Gamma_c)$. Second, the equilibrium between the monomer and micelle chemical potentials can be disrupted if the dissociation kinetics is hindered. As an example consider a bulk concentration above the CMC which is suddenly diluted to a value below the CMC. If the dissociation kinetics is slow then micelles will coexist with monomers seen at bulk concentrations below the CMC.

For completeness we discuss another important regime where kinetic barriers are absent. It has been shown by Stebe & Maldarelli (1994) that if kinetic barriers do not hinder the adsorption/desorption processes between bulk and interface, nor the exchange between micelles and monomers, then micellar systems can support constant chemical potential regions in interfacial flows. The result is the creation of regions which are free of Marangoni stresses and where the surface tension is constant and equal to $\gamma(\Gamma_c)$. This is the so-called remobilization regime due to the removal of Marangoni stresses and the behaviour of the system as if it was clean, albeit at a lower value of the surface tension. In this diffusion-limited regime the surface concentration is in local equilibrium with the bulk sublayer concentration according to the adsorption isotherm described earlier. Such regimes have been investigated numerically for rising gas bubbles (see, for example, Wang, Papageorgiou & Maldarelli 1999, 2002). The present work does not specifically study this particular limit but instead we choose to include kinetic barriers in order to evaluate and predict behaviour that may not be observed in clean systems (equivalently remobilized systems where a uniform but lower surface tension would be present, at least in large domains). A different model needs to be used in the diffusion-limited regime and we leave this for the future.

To the best of our knowledge, models for the breakup of jets in the presence of surfactant at high concentrations, above the CMC, have not yet been examined in the literature; this issue is addressed in the present paper. The question of being above or below the CMC and being able to model the surfactant dynamics coupled with the fluid mechanics is fundamental not just in jet breakup, but also in many other areas of interfacial fluid mechanics. We develop a long-wave model for the jet dynamics that comprises evolution equations for the interface, the axial velocity component and the interfacial, monomer and micellar surfactant concentrations; the model is closed by an appropriate surfactant equation of state. This work builds on that of Edmonstone, Craster & Matar (2006) carried out on the spreading of surfactant on thin liquid films above the CMC. The extended model developed here accounts for Marangoni stresses, surface and bulk diffusion, sorption kinetics and micellar formation and breakup kinetics. This model reduces to that of Craster *et al.* (2002)

for a jet covered with an insoluble surfactant in the appropriate limits. We demonstrate through a parametric study that the presence of surfactant at high concentration alters qualitatively the breakup dynamics and the formation of satellites. This will serve to motivate fully nonlinear two-dimensional simulations and experimental work to investigate the predictions and mechanisms that we describe.

The rest of this paper is organized as follows: The issues related to the presence of micelles, discussed above, are discussed in § 2. In this section, we provide details of the model formulation and pay particular attention to the choice of surfactant equation of state and its behaviour at high concentrations. The results of our parametric study are discussed in § 3 and, finally, concluding remarks are given in § 4.

2. Formulation

2.1. *Governing equations*

We consider the dynamics of a Newtonian and incompressible thread of an initially constant radius $\mathscr{R}$, of viscosity μ and density ρ. The thread is laden with surfactant, which is present at potentially high concentrations that exceed the CMC; the presence of surfactant influences the capillary-driven breakup of the thread. We use cylindrical coordinates (r, z) to describe the axisymmetric thread evolution: $r = 0$ and $r = S$ locate the thread axis and the interface, respectively; the gas overlying the thread is assumed to be inviscid.

The dynamics are governed by the following equations:

$$\nabla \cdot \boldsymbol{u} = 0, \tag{2.1}$$

$$\rho\,(\boldsymbol{u}_t + \boldsymbol{u} \cdot \nabla \boldsymbol{u}) = -\nabla p + \mu \nabla^2 \boldsymbol{u}, \tag{2.2}$$

$$\Gamma_t + \nabla_s \cdot (\boldsymbol{u}_s \Gamma) + \Gamma \boldsymbol{n} \cdot (\nabla_s \cdot \boldsymbol{n})\, \boldsymbol{u} = \mathscr{D}_s \nabla_s^2 \Gamma + J_{\Gamma c}, \tag{2.3}$$

$$c_t + \boldsymbol{u} \cdot \nabla c = \mathscr{D}_b \nabla^2 c - n J_{cm}, \tag{2.4}$$

$$m_t + \boldsymbol{u} \cdot \nabla m = \mathscr{D}_m \nabla^2 m + J_{cm}, \tag{2.5}$$

Equations (2.1)–(2.5) represent the equations of mass and momentum conservation, convective-diffusion equations for Γ, c and m, the surfactant concentrations at the interface, and in the bulk as monomers and micelles (comprising n monomers), respectively. Here, $\boldsymbol{u} = (u, w)$ is the velocity field in which u and w are its radial and axial components, respectively, p represents pressure and t denotes time; $\mathscr{D}_s$, $\mathscr{D}_b$ and $\mathscr{D}_m$ represent diffusion coefficients for the interfacial, monomer and micellar species, respectively; $\nabla_s = (\boldsymbol{I} - \boldsymbol{nn}) \cdot \nabla$ wherein $\boldsymbol{n} = (-S_z, 1)/(1 + S_z^2)$ is the outward pointing normal and $\boldsymbol{I}$ is the identity tensor.

The exchange between the different phases proceeds as follows. Firstly, at the interface

$$s + c' \underset{k_2}{\overset{k_1}{\rightleftharpoons}} \Gamma' \tag{2.6}$$

which represents the transfer of a surface molecule Γ', into the bulk phase c', thus creating a space s, at the free surface or conversely a monomer from the bulk using up a space at the interface; this model leads, at equilibrium, to the Langmuir isotherm and accounts for an effect, important at high concentrations, which is that the interfacial surfactant monomer may fully pack the interface. Implicit in the model is that the total space at the interface is limited. Secondly, the micelles and bulk

monomer are related via

$$nc' \underset{k_4}{\overset{k_3}{\rightleftharpoons}} m' \tag{2.7}$$

which represents the creation of a micelle m', in the bulk phase from n free bulk surfactant molecules, or the breakup of a micelle into n bulk monomers.

These relations carry with them certain implicit and natural assumptions. For instance, it is assumed that the micelles do not adsorb directly onto the interface, but that they must completely disassociate first into bulk monomers. It is also assumed that there is a strongly preferred micelle size n, which is indeed often the case in reality (Hunter 1991) and so the micelles are monodisperse.

The associations represented in (2.6) and (2.7) are turned into fluxes using the law of mass action to give $J_{\Gamma c}$ and J_{cm} as

$$\begin{aligned} J_{\Gamma c} &= k_1 c\left(1-\frac{\Gamma}{\Gamma_\infty}\right) - k_2\Gamma \text{ at } r = S(z,t), \\ J_{cm} &= k_3 c^n - k_4 m; \end{aligned} \tag{2.8}$$

these represent the sorptive flux at the interface $J_{\Gamma c}$ and a flux that controls the breakup and formation of micelles J_{cm}. This is the model utilized by Edmonstone *et al.* (2006) in their study of surfactant-laden droplet spreading above the CMC in which trends followed by experiment and theory were shown to be in qualitative agreement. The success of that modelling motivates the use of the fluxes and dynamic coupling with the fluid dynamics in the present context. It is worth noting that the methodology adopted above would allow one to incorporate different micellar models through these flux terms if desired.

The boundary conditions at $r = S(z,t)$ are

$$[\boldsymbol{n}\cdot\boldsymbol{T}\cdot\boldsymbol{n}] = \gamma\kappa, \quad [\boldsymbol{n}\cdot\boldsymbol{T}\cdot\boldsymbol{n}] = \mathbf{t}\cdot\nabla_s\gamma, \quad S_t + wS_z = u, \tag{2.9}$$

where κ is the interfacial curvature

$$\kappa = \frac{1}{S\left(1+S_z^2\right)^{1/2}} - \frac{S_{zz}}{\left(1+S_z^2\right)^{3/2}}. \tag{2.10}$$

Here, $\boldsymbol{T} = -p\boldsymbol{I} + \mu(\nabla\boldsymbol{u} + \nabla\boldsymbol{u}^T)$ is the stress tensor, and γ represents surface tension. At the interface, the following conditions hold for the monomers and micelles:

$$-\mathscr{D}_b(\boldsymbol{n}\cdot\nabla c) = J_{\Gamma c}, \quad \mathscr{D}_m(\boldsymbol{n}\cdot\nabla m) = 0. \tag{2.11}$$

Notably, these implicitly assume that the micelles must break down into bulk monomers before they are absorbed at the interface. Finally, at $r = 0$, we demand regularity.

The total mass of surfactant M is given by

$$M = 2\pi\int_0^L\int_0^S r(c+nm)\,\mathrm{d}r\,\mathrm{d}z + 2\pi\int_0^L S\Gamma\,\mathrm{d}z, \tag{2.12}$$

where L is the domain length.

2.2. *Equations of state*

In order to close the governing equations and boundary conditions, it is necessary to specify a surfactant equation of state, which incorporates the dependence of the surface tension γ on the surfactant interfacial concentration Γ. It is essential for this

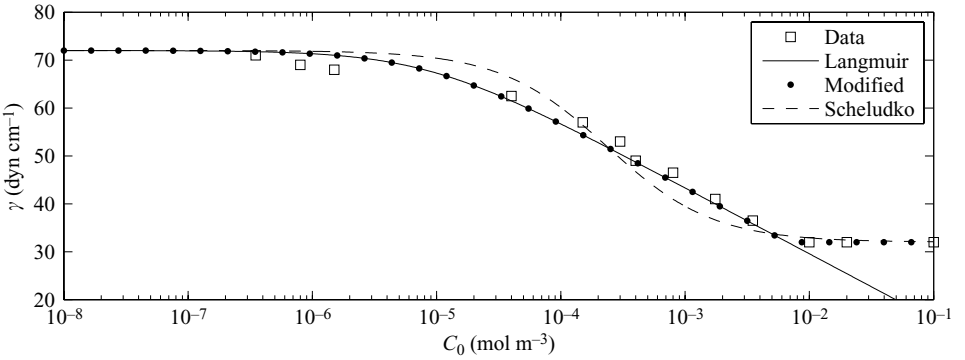

FIGURE 1. An illustration of the equations of state versus experimental data (squares), taken from Song *et al.* (2006). Notably the Langmuir model does not capture the plateau behaviour at high concentrations; the modified law (2.14) does so, as does the Sheludko model.

equation to be nonlinear since the interfacial concentration approaches and exceeds the one associated with maximal packing.

The Langmuir and Frumkin equations of state are given by

$$\gamma = \gamma_0 + R_g T \Gamma_\infty \left[\ln\left(1 - \frac{\Gamma}{\Gamma_\infty}\right) + \frac{1}{2} K \left(\frac{\Gamma}{\Gamma_\infty}\right)\right], \tag{2.13}$$

where T is the temperature, Γ_∞ the maximal packing concentration, R_g the universal gas constant and γ_0 the surface tension of a surfactant-free interface. The constant K ($=0$ for Langmuir and $\neq 0$ for Frumkin) gives a measure of any repulsion (>0) or attraction (<0) between the individual monomers on the surface. Experimental studies, for instance the data for the surfactant polyoxyethylene alkyl ethers $C_{14}E_6$ shown in figure 1 (Song *et al.* 2006), show that the Langmuir or Frumkin laws fit the data well over the majority of the concentration range.

However, there is a glaring issue as $\Gamma \to \Gamma_\infty$ with the Langmuir equation of state giving unphysically negative and ultimately divergent surface tension values. The experiments show a plateau in surface tension above $\Gamma = \Gamma_c$, where for the Langmuir model

$$\frac{\Gamma_c}{\Gamma_\infty} = 1 - \exp\left(\frac{\gamma_c - \gamma_o}{R_g T \Gamma_\infty}\right), \tag{2.14}$$

such that $\gamma = \gamma_c$ for $\Gamma > \Gamma_c$. Therefore we adopt a modified Langmuir equation of state which has γ given by (2.13) for $\Gamma < \Gamma_c$ and by γ_c for $\Gamma > \Gamma_c$. An illustration of this law, together with data and the conventional Langmuir fit from Song *et al.* (2006), is shown in figure 1. The parameters take the values $R_g = 8.314$ J K^{-1}mol^{-1}, $T = 300$ K, $\Gamma_\infty = 2.4 \times 10^{-6}$ mol m^{-2}, $\gamma_0 = 72$ dyn cm^{-1}, $\gamma_c = 32$ dyn cm^{-1} and $R = 10^6/8.35$ m^3 mol^{-1} in the dimensional equilibrium equation connecting bulk monomers and interfacial monomers. The Frumkin model is also compared to the data in Song *et al.* (2006) and it provides a minor improvement to the data fit, but it is not substantially different in character to merit further consideration here.

The Langmuir model, and its Frumkin cousin, are not the only equations of state that one could use. The Sheludko model is also popular

$$\gamma = \frac{\gamma_0}{(1 + \theta\Gamma/\Gamma_\infty)^3}, \quad \theta = (\gamma_o/\gamma_c)^{1/3} - 1$$

as it naturally asymptotes to the maximal surface tension value. For comparison it too is illustrated in figure 1. The fit is poor, for this surfactant data ($R = 2.5\times10^3$ m^3 mol^{-1} is taken to improve the fit), but it has provided an excellent data fit for several other surfactants, notably the oleic acid experiments of Gaver III & Grotberg (1992); we do not utilize this equation of state further in this paper.

2.3. *Scaling and long-wave asymptotics*

The governing equations, boundary conditions and surface equation of state are rendered dimensionless using the following scaling:

$$(r, S) = \mathscr{R}(\tilde{r}, \tilde{S}), \quad z = \mathscr{L}\tilde{z}, \quad (u, w) = V\left(1, \frac{\mathscr{L}}{\mathscr{R}}\right)(\tilde{u}, \tilde{w}), \quad t = \left(\frac{\mathscr{R}}{V}\right)\tilde{t}, \quad p = \left(\frac{\gamma_o}{\mathscr{R}}\right)\tilde{p},$$

$$\Gamma = \Gamma_\infty\tilde{\Gamma}, \quad c = c_{CMC}\tilde{c}, \quad m = \left(\frac{c_{CMC}}{n}\right)\tilde{m}, \quad \gamma = \gamma_o\tilde{\gamma},$$

$$J_{\Gamma c} = \left(\frac{V\Gamma_\infty}{\mathscr{R}}\right)\tilde{J}_{\Gamma c}, \quad J_{cm} = \left(\frac{Vc_{CMC}}{\mathscr{R}}\right)\tilde{J}_{cm}, \quad M = 2\pi\mathscr{R}^2\mathscr{L}\Gamma_\infty\tilde{M}, \tag{2.15}$$

where $\mathscr{L}$ and $V \equiv \gamma_o/\mu$ are characteristic length and velocity, respectively; we also define $\epsilon \equiv \mathscr{R}/\mathscr{L} \ll 1$. The tildes are suppressed henceforth.

We expand the flow variables and surfactant concentrations in powers of ϵ and the leading-order equations are given by (decorations designating leading-order quantities have been suppressed)

$$\frac{(ru)_r}{r} + w_z = 0, \quad p_r = \left[\frac{(ru)_r}{r}\right]_r, \quad \frac{(rw_r)_r}{r} = 0, \tag{2.16}$$

$$\Gamma_t + \frac{(Sw\Gamma)_z}{S} + \frac{\Gamma(u - wS_z)}{S} = \frac{1}{Pe_s}\frac{(S\Gamma_z)_z}{S} + J_{\Gamma c}, \tag{2.17}$$

$$c_t + uc_r + wc_z = \frac{1}{\epsilon^2 Pe_b}\left[\frac{1}{r}(rc_r)_r + \epsilon^2 c_{zz}\right] - J_{cm}, \tag{2.18}$$

$$m_t + um_r + wm_z = \frac{1}{\epsilon^2 Pe_m}\left[\frac{1}{r}(rm_r)_r + \epsilon^2 m_{zz}\right] + J_{cm}, \tag{2.19}$$

where we have set $Re = \epsilon^2\widehat{Re}$. Here, $(Pe_s, Pe_b, Pe_m) \equiv (V\mathscr{L}^2/\mathscr{R})(1/\mathscr{D}_s, 1/\mathscr{D}_b, 1/\mathscr{D}_m)$ are Peclet numbers and the fluxes read

$$J_{\Gamma c} = k_s\left[Rc(1-\Gamma) - \Gamma\right], \text{ at } r = S, \quad J_{cm} = k_m(c^n - m), \tag{2.20}$$

where the dimensionless parameters are

$$k_s \equiv k_2\mathscr{R}/V, \quad R \equiv k_1 c_{CMC}/k_2\Gamma_\infty, \quad k_m \equiv k_4\mathscr{R}/V \quad c_{CMC} \equiv (k_4/nk_3)^{1/(n-1)}. \tag{2.21}$$

At $r = S$, we have the following leading-order boundary conditions:

$$-p + 2(u_r - w_r S_z) = -\gamma\kappa, \quad w_r = 0, \quad S_t + wS_z = u, \tag{2.22}$$

with the non-dimensional curvature as

$$\kappa = \frac{1}{S\left(1+\epsilon^2 S_z^2\right)^{1/2}} - \frac{\epsilon^2 S_{zz}}{\left(1+\epsilon^2 S_z^2\right)^{3/2}}, \tag{2.23}$$

that is, we retain the full surface curvature. This is a standard device used in the literature (see, for instance, Eggers 1997; Craster *et al.* 2002) to both aid the stability

of computations and to introduce the physically important high wavenumber cutoff. The flux conditions at $r = S(z,t)$ are given by

$$-c_r + \epsilon^2 S_z c_z = \epsilon^2 Pe_b \beta J_{\Gamma c}, \quad m_r - \epsilon^2 S_z m_z = 0, \tag{2.24}$$

where

$$\beta = \Gamma_\infty / \mathscr{R} c_{CMC} \tag{2.25}$$

gives a measure of solubility. The dimensionless leading-order surfactant equation of state is given by

$$\begin{aligned} \gamma &= 1 + \Sigma \ln(1-\Gamma) \quad \text{for} \quad \Gamma < \Gamma_c, \\ &= \gamma_c \qquad\qquad\quad \text{for} \quad \Gamma \geqslant \Gamma_c, \end{aligned} \tag{2.26}$$

where $\Sigma \equiv R_g T \Gamma_\infty / \gamma_o$ and $\Gamma_c = 1 - \exp([\gamma_c - 1]/\Sigma)$ represent a surface elasticity parameter and the critical value of the surfactant interfacial concentration above which the surface tension remains equal to γ_c. The dimensionless total mass of surfactant reads

$$M = \int_0^L \int_0^S \frac{r}{\beta}(c+m)\,\mathrm{d}r\,\mathrm{d}z + \int_0^L S\Gamma\,\mathrm{d}z. \tag{2.27}$$

The following $O(\epsilon^2)$ equations are also required:

$$\widehat{Re}(w_t + u w_r + w w_z) = -p_z + w_{zz} + \frac{(r w_{1r})_r}{r}, \tag{2.28}$$

$$2(u_r - w_z)S_z + u_z + w_{1r} = \gamma_z, \ \text{at } r = S. \tag{2.29}$$

Here, w_1 denotes the $O(\epsilon^2)$ axial velocity component.

Following a procedure similar to that employed by Craster *et al.* (2002), the equations governing the evolution of S, w and Γ are easily found to be

$$S_t + w S_z + \tfrac{1}{2} w_z S = 0, \tag{2.30}$$

$$\widehat{Re}(w_t + w w_z) - 3w_{zz} - \frac{6 w_z S_z}{S} + (\gamma\kappa)_z - \frac{2\gamma_z}{S} = 0, \tag{2.31}$$

$$\Gamma_t + w\Gamma_z + \frac{\Gamma}{2} w_z = \frac{1}{Pe_s}\frac{1}{S}(S\Gamma_z)_z + k_s(Rc(1-\Gamma) - \Gamma). \tag{2.32}$$

These equations reduce to those derived by Craster *et al.* (2002) in the limit $k_s \to 0$ for which the surfactant is treated as insoluble. In order to derive similar equations for c and m, we adapt below a procedure previously employed in studying surfactant-driven thin films as in Jensen & Grotberg (1993) and Edmonstone *et al.* (2006).

2.4. *Cross-sectional averaging*

We assume that radial diffusion is rapid and consequently that $\epsilon^2(Pe_b, Pe_m) \ll 1$. We set $(c, m) = (c_0, m_0)(z,t) + \epsilon^2(Pe_b, Pe_m)(c_1, m_1)(r,z,t)$ where

$$\frac{1}{\pi S^2}\int_0^S 2\pi r (c_1, m_1)\,\mathrm{d}r = 0. \tag{2.33}$$

As a result of the above decomposition, we have

$$c_{0t} + w c_{0z} = \frac{1}{r}(r c_{1r})_r + \frac{1}{Pe_b} c_{0zz} - k_m\left(c_0^n - m_0\right), \tag{2.34}$$

and the following condition at $r = S$

$$c_{1r} = \frac{1}{Pe_b} S_z c_{0z} - \beta J_{\Gamma c}. \tag{2.35}$$

Cross-sectional averaging of (2.34) and using (2.35) yields the following evolution equation for c_0:

$$c_{0t} + w c_{0z} = \frac{1}{S^2 Pe_b} \left(S^2 c_{0z}\right)_z - \frac{2\beta}{S} J_{\Gamma c} - k_m \left(c_0^n - m_0\right). \tag{2.36}$$

Using a similar procedure, we have the following evolution equation for m_0:

$$m_{0t} + w m_{0z} = \frac{1}{S^2 Pe_m} \left(S^2 m_{0z}\right)_z + J_{cm}. \tag{2.37}$$

The breakup dynamics are governed by (2.30)–(2.32), (2.36) and (2.37) coupled with the fluxes defined in (2.20). In what follows, the subscript '0' is suppressed.

We scale out $\widehat{Re}$ by making the following changes of variables and rescalings:

$$S = \widehat{Re}\hat{S}, \quad t = \widehat{Re}\hat{t}, \quad w = \frac{1}{\widehat{Re}}\hat{w},$$

$$\hat{\epsilon} = \epsilon \widehat{Re}, \quad \frac{1}{\widehat{Pe}_i} = \frac{\widehat{Re}}{Pe_i}, \quad \hat{k}_i = \widehat{Re} k_s, \quad \hat{\beta} = \frac{\beta}{\widehat{Re}} \tag{2.38}$$

which finally yields the following evolution equations (after dropping the hat decoration):

$$S_t + w S_z + \tfrac{1}{2} w_z S = 0, \tag{2.39}$$

$$(w_t + w w_z) - 3 w_{zz} - \frac{6 w_z S_z}{S} + (\gamma \kappa)_z - \frac{2\gamma_z}{S} = 0, \tag{2.40}$$

$$\Gamma_t + w\Gamma_z + \frac{\Gamma}{2} w_z = \frac{1}{Pe_s} \frac{1}{S} (S\Gamma_z)_z + k_s (Rc(1-\Gamma) - \Gamma), \tag{2.41}$$

$$c_t + w c_z = \frac{1}{S^2 Pe_b} \left(S^2 c_z\right)_z - \frac{2\beta}{S} k_s (Rc(1-\Gamma) - \Gamma) - k_m (c^n - m), \tag{2.42}$$

$$m_t + w m_z = \frac{1}{S^2 Pe_m} (S^2 m_z)_z + k_m (c^n - m). \tag{2.43}$$

Owing to the scaling on β, the mass of surfactant is unaffected by this rescaling and remains as

$$M = \int_0^L \left(\frac{S^2}{2\beta} (c + m) + S\Gamma \right) \mathrm{d}z. \tag{2.44}$$

These involve the equation of state, γ, from § 2.2 and the curvature, κ, from (2.23).

2.5. *Equilibrium*

The most natural initial conditions are those of equilibrium where $J_{\Gamma c} = J_{cm} = 0$. This condition, subject to the mass of surfactant constraint, gives

$$\frac{M}{L} = \frac{1}{2\beta} \left(c_o + c_o^n\right) + \frac{Rc_o}{1 + Rc_o}, \tag{2.45}$$

with $m_o = c_o^n$ and

$$\Gamma_o = \frac{Rc_o}{1 + Rc_o}. \tag{2.46}$$

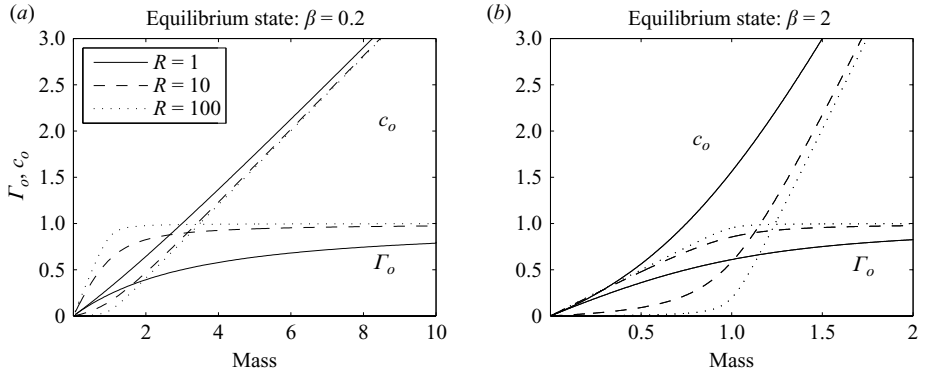

FIGURE 2. The equilibrium states, in the absence of micelles, for (*a*) highly soluble monomers, $\beta = 0.2$, and (*b*) weakly soluble monomers, $\beta = 2$, for $R = 1, 10, 100$.

In the absence of micelles,

$$\frac{M}{L} = \frac{1}{2\beta} c_o + \frac{R c_o}{1 + R c_o}, \tag{2.47}$$

with Γ_o given by (2.46), and typical equilibrium values are shown in figure 2. This figure illustrates the physical importance of R; this parameterizes, for a fixed solubility β, the attraction of the interface to surfactant monomers with large R corresponding to a strong affinity to the interface. It is notable that once the non-dimensional mass rises above unity, then as R increases the interfacial surfactant concentration approaches maximal packing. Low values of R require much higher mass concentrations before this becomes evident.

The parameter β quantifies the relation between the maximal packing interfacial surfactant concentration and the bulk concentration at which micelles are formed, i.e. it is a measure of the solubility with $\beta \ll 1$ being highly soluble and $\beta \gg 1$ nearly insoluble.

Much larger mass concentrations mean that one enters a situation where micelle formation becomes inevitable. The additional micelle species is characterized by the micelle size n of which $n \geqslant 10$ is typical. The resulting equilibrium states are shown in figure 3 for highly soluble and less soluble monomers. Interesting limits include $R \gg 1$ and $\beta \gg 1$ (attracted to the interface and weakly soluble) which ensure that the monomers remain mainly at the interface until the available mass exceeds β, thereafter monomers must accumulate in the bulk and form micelles. An example of this behaviour is shown by the dotted curves in figure 3(*b*, *d*, *f*). The more soluble case, figure 3(*a*, *c*, *e*), readily forms micelles at lower mass concentrations and apart from the interfacial concentration Γ, the surfactant is dominated by the micellar species through $m_o = c_o^n$; in all cases the micelle concentration is effectively zero until $c_o \to 1$, i.e. as the critical micelle concentration is approached when their formation is rapid and their concentration increases strongly; this is in line with the physical chemistry where experiments show rapid transitions once the CMC is exceeded. The bulk concentration c_o now naturally asymptotes to a value close to unity, as the available surfactant mass increases, unlike the behaviour shown in figure 2, with the excess bulk monomers now absorbed into a reservoir of micelles.

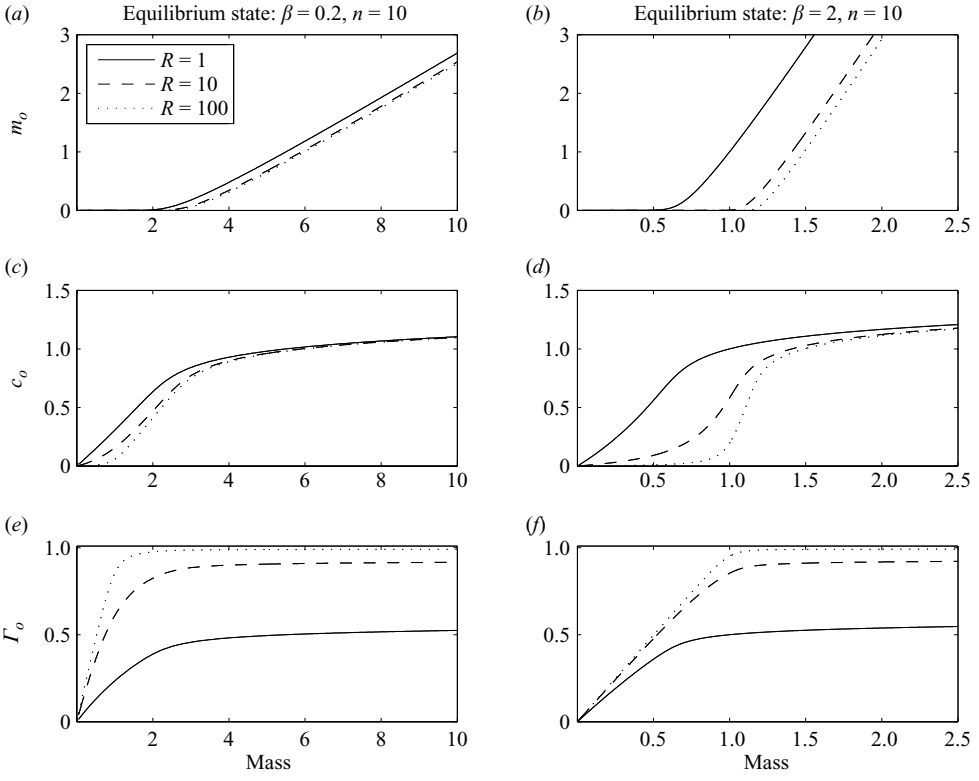

FIGURE 3. The equilibrium states in the presence of micelles, $n = 10$, for (a, c, e) highly soluble monomers $\beta = 0.2$ and (b, d, f) less soluble monomers $\beta = 2$, for $R = 1, 10, 100$.

3. Discussion of results

In this section, we present a discussion of the results of the parametric study.

3.1. *Numerical simulations*

The system of coupled highly nonlinear partial differential equations (2.39)–(2.43) is solved numerically using the highly efficient PDE solver EPDCOL (Keast & Muir 1991). This numerical routine, which utilizes finite-elements to discretize the spatial derivatives and Gear's method in time, has been previously used to study the breakup of single and compound jets by Craster *et al.* (2002) and Craster, Matar & Papageorgiou (2005). The numerical predictions were validated against those of another routine, based on the finite-difference approximation in space (Craster & Matar 2007), as well as against the predictions of linear theory.

Typically, 6000 grid points were used to carry out the computations with convergence being achieved upon mesh refinement; we have also ensured that mass is conserved to within 0.1 % in all computations. The simulations were halted as breakup is approached when S reached values of order 10^{-4} locally; beyond this point, spatial derivatives could no longer be resolved with sufficient accuracy.

Numerical solutions are determined starting from the following initial conditions:

$$S(z, 0) = \frac{10}{9}[1 - 0.1\cos(\pi z/5)],\ \Gamma = \Gamma_o,\ c = c_o,\ m = m_o,\ w = 0, \tag{3.1}$$

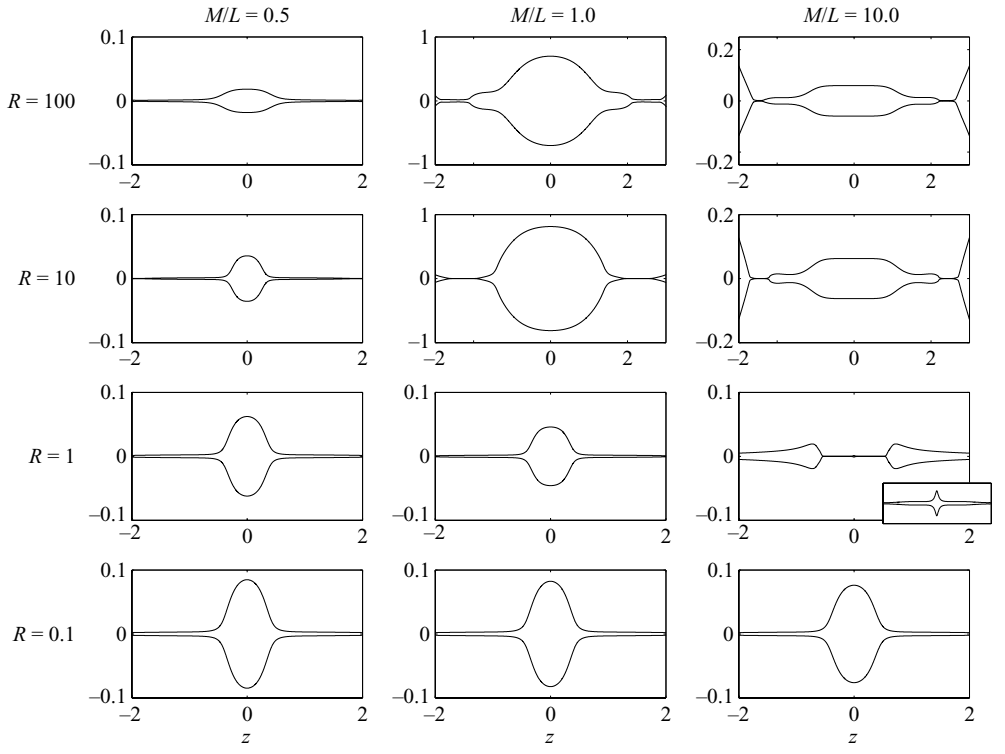

FIGURE 4. A 'phase diagram' in the $(R, M/L)$ space detailing the shape of the interface S (the reflection $-S$ is also shown to emphasize the axisymmetric character of the problem) immediately prior to breakup; note the variation in the vertical axis between the panels. The parameter R characterizes the attraction of surfactant to the interface and is fixed for each row, and M/L quantifies the amount of surfactant present and is fixed for each column. Here, $\beta = k_s = k_m = 1$, $\gamma_c = 0.4$ and $\epsilon = 0.01$. The inset to $M/L = 10$, $R = 1$ shows the creation of a very small satellite just before breakup in the central region.

in $-5 < L < 5$; these correspond to an initially motionless thread of slightly perturbed interface, containing surfactant under equilibrium conditions. The applied disturbance is chosen to be in the band of unstable wavenumbers found using linear theory. The solutions are obtained subject to the following boundary conditions:

$$w(\pm L, t) = 0, \quad S_z(\pm L, t) = S_{zzz}(\pm L, t) = 0, \quad \Gamma_z(\pm L, t) = c_z(\pm L, t) = m_z(\pm L, t) = 0. \tag{3.2}$$

Due to the parametric richness of the present problem, we focus on the physico-chemical parameters β, k_s, k_m, R, γ_c and M, whose effect on the breakup dynamics have not been previously explored extensively in the literature. The values of the Peclet numbers will be fixed for the remainder of this paper, $Pe_s = Pe_b = Pe_m = 10$, as will the values of the surface elasticity $\Sigma = 0.5$, the high-concentration surface tension plateau, $\gamma_c = 0.4$, and the aspect ratio, $\epsilon = 0.01$; the latter appears in the expression for the interfacial curvature. The 'base' case that will be studied below is parameterized by $\beta = k_s = k_m = M/L = 1$ and $n = 10$. The effect of each of these parameters, with the exception of n, on the dynamics will be explored.

In order to motivate the discussion of the results, we show in figure 4 a 'phase diagram' in $(R, M/L)$ space that demonstrates the effect of these parameters on the interfacial shape immediately prior to breakup; the rest of the parameters correspond

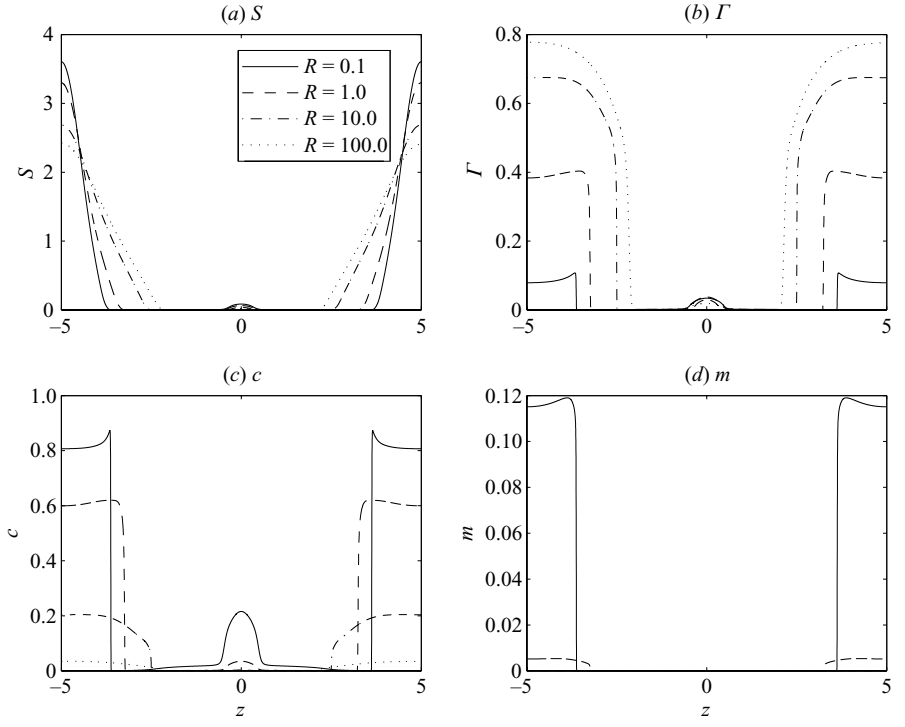

FIGURE 5. The effect of the attraction of surfactant to the interface R on interface position S, interfacial Γ, bulk c and micelle m concentrations, shown in (a)–(d) very close to breakup, that is when $S_{min} \sim 10^{-4}$. Here, $M/L = 0.5$ and the rest of the parameters remain unaltered from figure 4.

to the 'base' case. It is shown clearly that in the large majority of the cases studied, the breakup dynamics are accompanied by satellite formation. It is also notable that the cases represented by the parameters corresponding to the last row and first column (and $M/L = 1$, $R = 1$) give rise to relatively small satellites of roughly similar size. The cases represented by the parameters corresponding to the four satellites in $M/L = 1, 10$ and $R = 10, 100$ on the other hand, have markedly larger satellites and/or a different shape; the $M/L = 10$, $R = 1$ case has a satellite, which is almost indiscernible, as breakup is approached. We now explain the dynamics leading to these results, dividing the discussion into two subsections for the flow behaviour below the CMC ($M/L < 1$) and above it ($M/L > 1$).

3.2. *Lower than the CMC: $M/L < 1$*

Figure 5 shows the effect of varying R in the range $0.1 \leqslant R \leqslant 100$ on the profiles of S, Γ, c and m immediately prior to breakup with $M/L = 0.5$ and the rest of the parameters remain unchanged from the 'base' case. In all of the cases shown in figure 5, the thread thins at the flow origin under the action of capillary forces that act to minimize its interfacial area, ultimately leading to breakup. The flow is accompanied by the rapid transport of surfactant away from the thinning region and the formation of surfactant-laden satellite drops during its latter stages. The range of R considered spans the full spectrum of surfactant behaviour: at low R values, the surfactant has a preference for micellar formation; high R values are associated with an affinity for the interface and low micelle concentrations, as shown in figure 5(b–d).

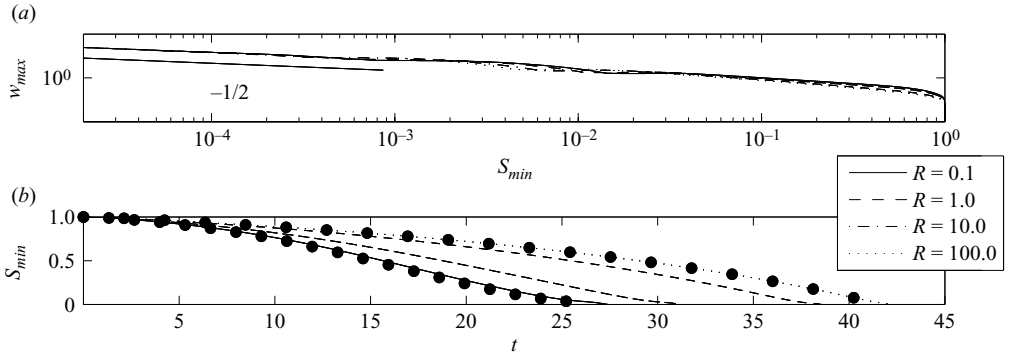

FIGURE 6. The effect of attraction of surfactant to the interface R on the temporal variation of w_{max}, (a) the maximal axial velocity, (b) the minimal interfacial radius S_{min}. Also shown in (a) is a line of constant slope equal to $-1/2$, which represents the dynamics expected from a balance between inertial, capillary and viscous forces as breakup is approached (Eggers 1997), that is as $\tau = t_b - t \to 0$ where t_b is an estimate of the breakup time. The filled circles in (b) designate the minimal thickness for the surfactant-free and insoluble surfactant cases. The rest of the parameters remain unaltered from figure 5.

The axial velocity increases progressively in the breakup region as depicted by figure 6(a). This is to be expected since the velocity rises beneath the thinned region due to the increase in capillary pressure there. Scalings for S, w and z in the surfactant-free case can be obtained by balancing inertia, the capillary pressure gradient and viscous retardation in (2.39) and (2.40): $z \sim \tau^{1/2}$, $S \sim \tau$ and $w \sim \tau^{-1/2}$ as $\tau = t_b - t \to 0$ where t_b is an estimate of the breakup time Eggers (1997). So that the dynamics evolve towards these scalings for the case of insoluble surfactant has been previously confirmed (Craster *et al.* 2002). Close inspection of figure 6(a) reveals that these scalings are also approached in the present case for all R values examined due to the 'sweeping' of the surfactant away from the thinning region. Notable in figure 5 (b)–(d) are steep gradients in the surfactant concentrations near the point of pinch-off, the surfactant is swept out to relatively stagnant zones where it accumulates unable to escape; when viewed in dimensional terms the gradients are not as severe as they appear in the current scaling.

The evolution of the thread for $R = 0.1$ resembles that associated with the surfactant-free case, as shown in figure 6(b), in which the temporal evolution of the minimal thread radius is plotted; the dynamics of the surfactant-free case are computed by solving (2.39) and (2.40) with $\gamma = 1$. This observation also explains the weak variation in the final satellite shape in the last row of figure 4: despite the increase in the total surfactant mass, only a relatively small fraction of this is transported to the interface. The $R = 100$ case mimics closely that of a thread covered with an insoluble surfactant, obtained via solution of (2.39)–(2.41) with $k_s = 0$, as also shown in figure 6(b). For R between the two extreme cases, increasing R retards the evolution towards breakup and gives rise to smaller satellite drops (see figure 7a). This is due to an associated increase in the relative significance of Marangoni stresses that induce flow from low-γ (either side of the thinning region) to high-γ regions (the thinning region), which counteracts the capillary-driven thinning. The surfactant monomer concentration in the bulk, c, approaches the dynamic equilibrium with $c \approx \Gamma/(R(1-\Gamma))$.

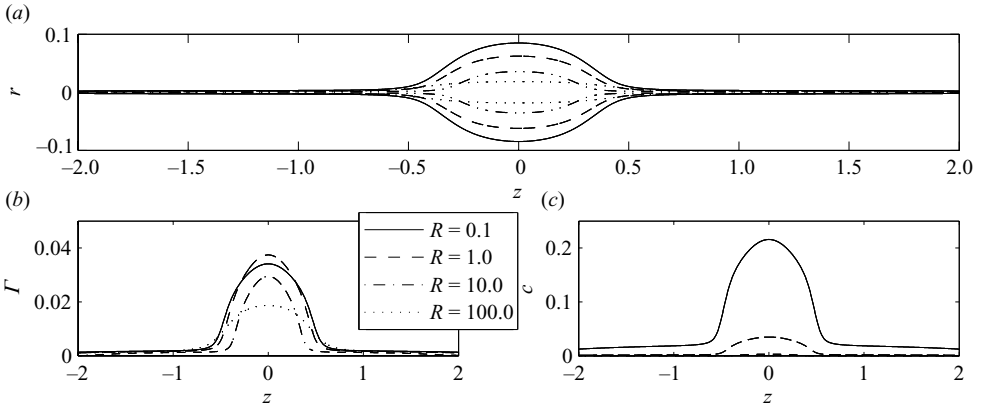

FIGURE 7. The satellite drop shape (S and $-S$) is shown in (a) as the attraction parameter R varies. (b) and (c) show the profiles of interfacial Γ and bulk c surfactant. These are all shown at times immediately prior to breakup.

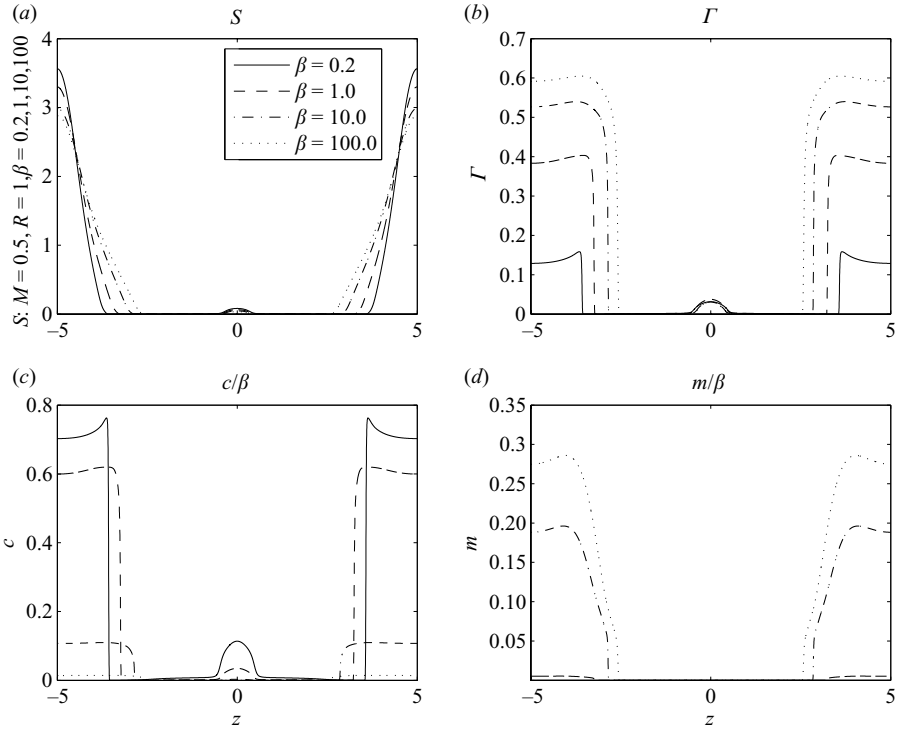

FIGURE 8. The effect of solubility β on interfacial position S, interfacial Γ, bulk c and micelle m, surfactant concentrations shown in (a)–(d) very close to breakup where $S_{min} \sim 10^{-4}$. Here, $M/L = 0.5$ and the rest of the parameters remain unaltered from figure 4.

The effect of surfactant solubility, parameterized by β, on the breakup dynamics is also of interest. Figures 8 and 9, are essentially equivalent to figures 5–7 that showed the effect of R; here $R = 1$ and the rest of the parameters take their 'base' case values. One notes a correspondence between the trends observed in the two sets of figures: the case of a weakly (highly) soluble surfactant, characterized by large

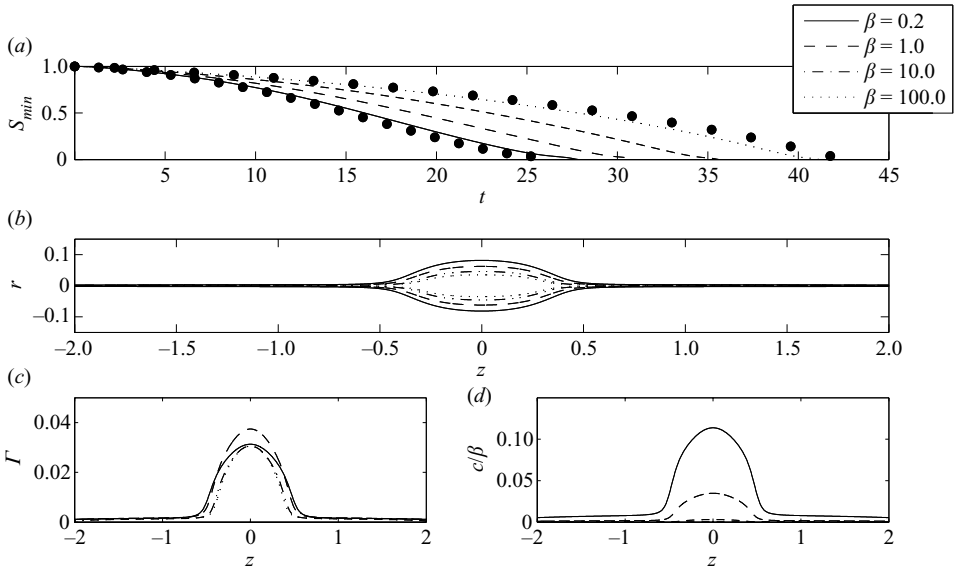

FIGURE 9. The effect of solubility β on the minimal interfacial radius S_{min} (a), and the satellite drop (S and $-S$) shape as well as the profiles of Γ and c immediately prior to breakup (b)–(d), respectively. The rest of the parameters remain unaltered from figure 8. The filled circles in (a) designate the minimal thickness for the surfactant-free and insoluble surfactant cases.

(small) β values, is associated with high (low) Γ values and large (small) Marangoni gradients that retard (accelerate) breakup and give rise to smaller (larger) satellite drops. The bulk surfactant concentrations, c and m, are shown normalized by β so that, if re-dimensionalized, these curves give the surfactant concentration relative to the maximal interfacial packing value (see figure 8(c, d)).

The nonlinear equation of state plays a minor role as the surfactant concentrations are rarely above the critical value ($\Gamma_c = 0.7$ for the parameters considered here), for which the surface tension plateau occurs. The only regions where this may occur in the present case are at the edges of the domain which are benign as far as the break-up and thinning processes are concerned. We have also found the results to be weakly dependent on k_s and k_m for $M/L < 1$.

3.3. *At and above the CMC: $M/L \geqslant 1$*

As the CMC is approached, we expect that the nonlinear equation of state featuring the surface tension plateau above the critical value Γ_c may play a role. The effect of varying R on the flow profiles immediately prior to breakup is shown in figure 10 for $M/L = 1$ and the rest of the parameters remaining at their 'base' values. It is clearly seen that whereas the profiles associated with $R = 0.1$ and $R = 1$ resemble closely those previously observed with $M/L = 0.5$, the profiles generated with $R = 10$ and $R = 100$ are distinctly different. The latter are characterized by much larger satellite drops with $\Gamma > \Gamma_c = 0.7$ over large proportions of the computational domain.

At such large values of R and with $M/L = 1$, there appears to be a sufficient mass of surfactant to 'flood' the interface with monomers, pushing the interfacial concentration beyond Γ_c and γ to γ_c. As a result, the thread undergoes breakup driven by an approximately uniform surface tension, in the absence of retarding Marangoni stresses. Then, after a sufficient amount of interfacial species has been swept away from the thinning region, Γ decreases locally below Γ_c and causing γ to

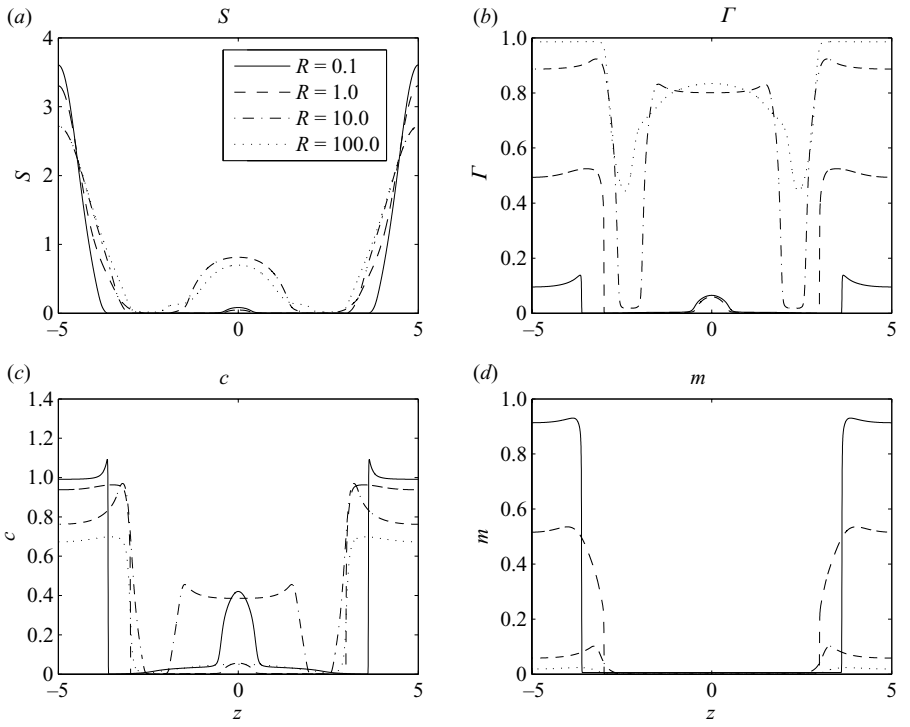

FIGURE 10. The effect of attraction of surfactant to the interface R on S, Γ, c and m, shown in (a)–(d) at times very close to breakup, that is when $S = 10^{-4}$. Here the mass of surfactant present is fixed as $M/L = 1$ and the rest of the parameters remain unaltered from figure 4.

rise above γ_c in the thinning region; this takes place at an earlier time in the dynamics at $R = 10$ and $R = 100$ than in the case of lower R values, at which the thread radius is relatively thick (this will be discussed further below in connection with figure 11a). The sudden local increase in γ drives Marangoni flow towards the thinning region, which leads to the formation of a much larger satellite drop than could be achieved with $R = 0.1, 1$. This provides a speculative explanation for the reasons underlying the results presented in the middle column of figure 4 which will be considered in more detail in § 3.4.

Figure 11(a) shows that although the overall trend is that an increase in R retards the thinning process, close inspection of this panel reveals the formation of a 'shoulder' in the S_{min} vs time plot for $R = 10$ and $R = 100$ at $t \approx 30$. We speculate at this juncture that this coincides with the time at which $\Gamma < \Gamma_c$ and $\gamma > \gamma_c$ local to the thinning region and the onset of the satellite-forming Marangoni-driven flow towards this region. It should be noted that the value of S_{min} at the onset of this flow is much larger than at the onset of satellite formation for $R = 0.1$ and $R = 1$. This is one of the main contributors to the large size of the satellite drops formed at high R values. We have also found that this size increases with increasing γ_c (not shown) since $\gamma > \gamma_c$ in the thinning region at an earlier time and for larger S_{min}.

As we head far above CMC, to $M/L = 10$, corresponding to the last column of figure 4, we find that the final satellite shapes for $R = 10, 100$ are smaller than those for $M/L = 1$ but significantly larger than those found when below CMC. The mechanism by which they are formed is identical to that for $M/L = 1$ except

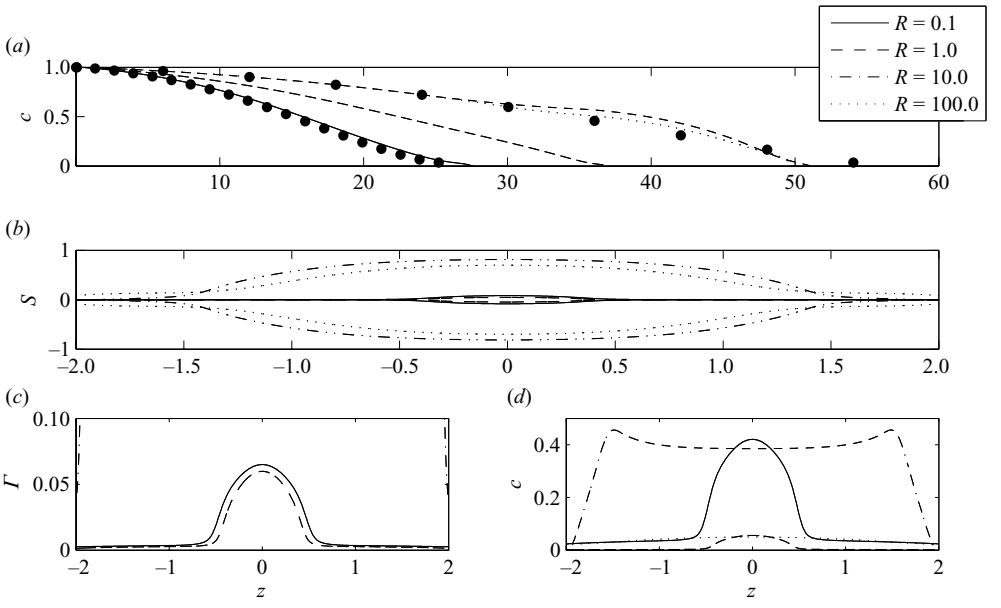

FIGURE 11. The effect of attraction of surfactant to the interface R on the minimal interfacial radius S_{min} (a), and the satellite drop shape (S and $-S$) as well as the profiles of interfacial Γ and bulk c surfactants immediately prior to breakup (b)–(d), respectively. The rest of the parameters remain unaltered from figure 10. The filled circles in (a) designate the minimal thickness for the surfactant-free and insoluble surfactant cases. In (c) the Γ profiles for $R = 10, 100$ are absent since they are off the scale.

that the reservoir of surfactant acts to moderate the effect of the nonlinear equation of state. The large values of R allow the surfactant to preferentially collect at the interface. Decreasing R leads, at $R = 0.1$, to the surfactant preferring the bulk and the surfactant plays a minor role in the dynamics. The intermediate case $R = 1$ is interesting as there is an interplay between surfactant replenishing the interface in the central region and the formation of the satellite, the result being that the satellite splits in half; this is interpreted in detail in § 3.4.

3.4. *Mechanisms for satellite formation*

In this section, we contrast the different mechanisms leading to the formation of the satellite drops shown in figure 4. The satellites fall into two classes: the bottom two rows and the left column for which the satellites are small; and the four satellites for $M/L = 1, 10$ and $R = 10, 100$ that are distinctly larger in size. We consider the 'small' satellites first.

The details of satellite formation for $M/L = 1$ and $R = 1$ are shown in figure 12 together with 'diagnostics' that help determine the underlying mechanism. It is notable that the satellite only forms just before breakup (cf. figure 12a), and is accompanied by a small rise in the interfacial concentration there. One can also decompose the axial fluid acceleration in (2.40) into its constituents, which are shown immediately prior to breakup in figure 12(c); also shown in this panel is the 'final' shape of the interface. It can be seen that inertia acts to decelerate the fluid in the neighbourhood of the origin. Although it is initially a small effect, it eventually creates the local flow reversal necessary for satellite formation. The surfactant distribution also creates a flow that opposes jet breakup: Marangoni flows are driven from regions of high

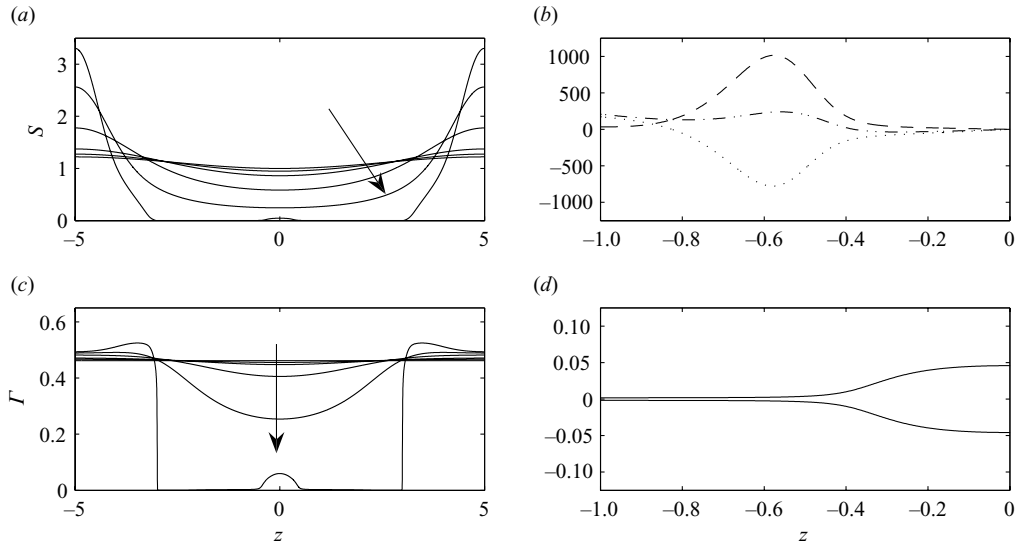

FIGURE 12. Satellite formation for surfactant mass, $M/L = 1$, and attraction $R = 1$, with the rest of the parameters remaining the same as in figure 4. (a) and (c) show the evolution of interface position S and interfacial surfactant Γ for times $t = 0.2, 0.5, 10, 20, 30$ and 37.02. In this, and subsequent figures, the arrows show the direction of increasing time. (b) shows the constituents of (2.40) at $t = 37.02$, that is, just before breakup: the acceleration term $-ww_z$ (dashed line), the sum of the remaining terms in the right-hand side of (2.40) (dotted line), and w_t (dot-dashed line). (d) shows the final satellite shape (S and $-S$) allowing one to see where the maximal acceleration terms shown in (b) are of maximum effect.

surfactant concentrations (at the edges of the domain and at the centre) into the thinned regions. These, however, merely act to delay rather than prevent the breakup event and decrease the size of satellite drops (as shown in figures 6b and 7a).

The larger satellites are created by effects due to the severe nonlinearity of the equation of state, in particular by the plateau in surface tension that occurs for $\Gamma > \Gamma_c$. The evolution of the flow profiles for the $M/L = 1$ and $R = 10$ case is shown in figure 13. Several features are striking, in particular the nonlinear equation of state relating γ to Γ forces a very sharp change in the surface tension. Thus if $\Gamma > \Gamma_c$ the surfactant dynamics are virtually irrelevant as the surface tension is constant. However, once enough surfactant has been swept away from the breakup region sufficiently rapidly that it cannot be replenished from the bulk via adsorption and Γ drops below Γ_c, then the surface tension locally increases and a Marangoni stress, Γ_z/S, decelerates the jet. This is best seen in figure 14(b) and its effect on S_{min} is evident in figure 14(c); the time, $t = 30$, is chosen to be just after Γ decreases beyond the critical value. There are two main differences between these satellites and the more conventional ones, discussed in the previous paragraph. First, inertia is irrelevant to the mechanism described; in fact, simulations (not shown) in the Stokes limit give virtually identical satellites. Secondly, the satellites form much earlier in time and their size is set by the sudden deceleration imposed by the Marangoni stresses. The point of similarity is that the satellites are created by localized decelerations that eventually cause local flow reversal.

Inspection of figure 4 reveals that the $M/L = 1, R = 10$ case has a much larger satellite than when $M/L = 10, R = 10$. It is interesting to briefly explore the mechanism behind this decrease. First, one notes that due to the enhanced mass

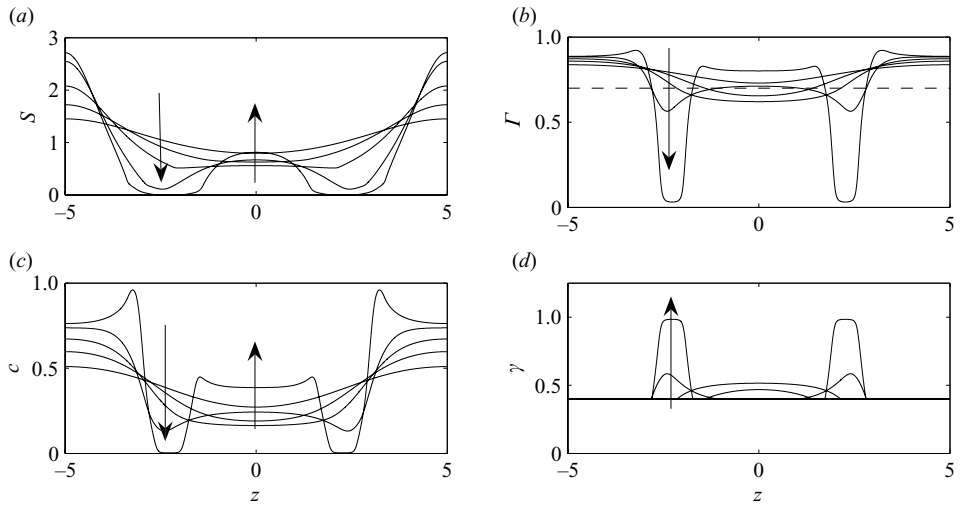

FIGURE 13. Satellite formation for $M/L = 1$ and $R = 10$ with the rest of the parameters remaining the same as in figure 4. (a)–(d) show the evolution of interface position S, interfacial Γ, bulk c surfactant and surface tension γ for times $t = 20, 30, 40, 48.6$ with the emergence of a large satellite evident even at early times.

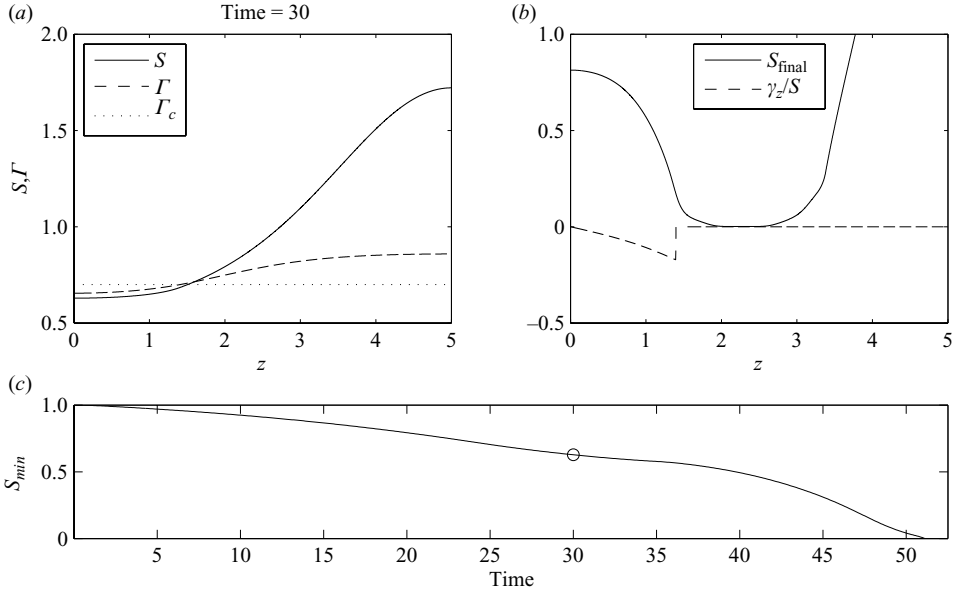

FIGURE 14. Satellite formation for $M/L = 1$ and $R = 10$ with the rest of the parameters remaining the same as in figure 4. (a) shows the profiles of S and Γ for $t = 30$ which is just after the interfacial surfactant Γ drops below the critical value Γ_c. (b) shows an enlarged view of final satellite profile and the Marangoni contribution to (2.40) at $t = 30$. (c) shows S_{min} versus time with $t = 30$ circled.

of surfactant the interfacial surfactant remains above the critical plateaux value, Γ_c, until late times. Thus the jet thins considerably before the deceleration due to Marangoni begins. In figure 15, we show S and Γ at $t = 53.9$, just after Γ drops below Γ_c; at this time, there is no satellite formation. However, the effect of the Marangoni

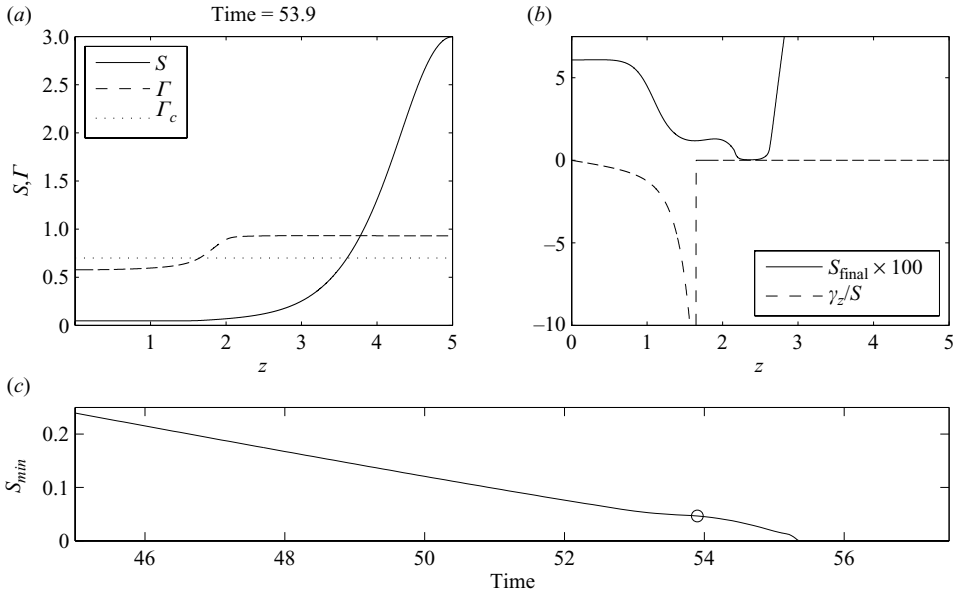

FIGURE 15. Satellite formation for $M/L = 10$ and $R = 10$ with the rest of the parameters remaining the same as in figure 4. (a) shows the profiles of S and Γ for $t = 53.9$ which is just after the interfacial surfactant Γ drops below the critical value Γ_c. (b) shows an enlarged view of final satellite profile and the Marangoni contribution to (2.40) at $t = 53.9$. (c) shows S_{min} versus time with $t = 53.9$ circled.

stresses on S_{min} is clear with the deceleration causing a slight kink in the curve at $t = 53.9$ (this is circled in the figure). The Marangoni stress for $t = 53.9$ is shown in figure 15 and this initial point of deceleration sets the final satellite size; a smaller protuberance is created by the slight movement of the maximum in Marangoni stress as time increases.

The case of $M/L = 10$ and $R = 1$ shown in figure 4 is interesting since the shape of the interface near the origin is markedly different from the other cases presented in this figure. Despite the relatively large mass of surfactant present, the interfacial surfactant concentration is not maintained above the critical plateau value Γ_c. This is because for $R = 1$ the surfactant prefers to remain within the bulk, and so strongly nonlinear effects from the equation of state do not play a role. The satellites form just before breakup occurs. The time scale for this final pinch-off event is illustrated in figure 16(a, b) that shows almost flat central portions at $t = 42.25$ and breakup at $t = 43.76$; the dynamics are not similar to the larger satellite formation process discussed previously.

Even though R is relatively small, there is a flux of surfactant from the bulk to the interface in the thinned region that weakly replenishes the surfactant there. This creates a local Marangoni stress that advects fluid away from the flow origin. This is shown in figure 16 for $t = 42.25$; the local additional acceleration correlates with the inner edge of the larger satellite. This creates local thinning near the origin and forces local breakup, which corresponds to a localized restarting of the breakup process but now for a much thinner jet with little surfactant present. The simulations yield a tiny localized satellite at the flow origin, as shown in figure 16(a). Although it is not possible to track the thread evolution beyond the point shown in figure 16, one

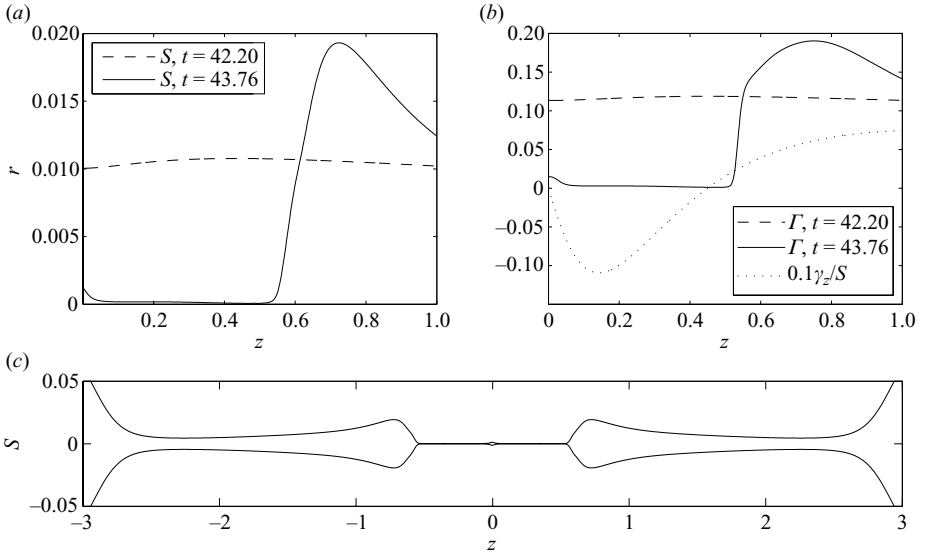

FIGURE 16. The near breakup behaviour for $M/L = 10$ and $R = 1$ with the rest of the parameters remaining the same as in figure 4. (a) and (b) show the profiles of interface position S and interfacial surfactant Γ for $t = 42.2, 43.76$ just as the satellites form and at breakup. (b) also shows the Marangoni contribution to (2.40) while (c) shows S and $-S$ to emphasize the axisymmetric nature of the final satellite shapes.

possible scenario involves breakup being accompanied by the formation of satellites that corresponds to the small drop at the origin and the larger bulges on either side of it; another scenario involves the retraction of the bulges into the main thread, leaving a small satellite at the origin.

4. Conclusions

We have studied the breakup of a thread laden with surfactant at high concentration above the CMC. A model for the breakup dynamics has been developed based on the long-wave approximation. This model comprises coupled evolution equations for the interface, the axial velocity component and the concentration of surfactant at the interface and in the bulk where it exists in the form of monomers and micelles (provided the concentration exceeds the CMC). A nonlinear equation of state is used for closure, which accounts for the formation of a surface tension plateau at high surfactant concentrations. The results of our numerical simulations demonstrate the formation of large satellites, which, at sufficiently high concentrations, and for surfactants with a strong affinity to the interface, are driven by Marangoni stresses. This is a markedly different mechanism to that usually required for satellite formation which requires inertial effects. The mechanism underlying the formation of the larger satellites is new and has not been commented on previously in the literature. There remains much to be explored in the interfacial mechanics of flows above the CMC and the model presented here provides a template for future studies and extensions, it is envisaged that this will provide motivation for fully three-dimensional axisymmetric nonlinear simulations and further experimental work.

DTP was supported in part by the National Science Foundation Grant DMS-0707339. OKM and RVC acknowledge support from the EPSRC through the platform grant EP/E046029/1. We are grateful to the referees for many helpful and constructive comments.

REFERENCES

Ambravaneswaran, B. & Basaran, O. A. 1999 Effects of surfactants on the nonlinear deformation and breakup of stretching liquid bridges. *Phys. Fluids* **11**, 997–1015.

Ambravaneswaran, B., Wilkes, E. D. & Basaran, O. A. 2002 Drop formation from a capillary tube: comparison of one-dimensional (1-d) and two-dimensional (2-d) analyses and occurrence of satellite drops. *Phys. Fluids* **14**, 2606–2621.

Anna, S. L., Bontoux, N. & Stone, H. A. 2003 Formation of dispersions using flow focusing in microchannels. *Appl. Phys. Lett*. **82**, 364–366.

Bazhlekov, I. B., Anderson, P. D. & Meijer, H. E. H. 2006 Numerical investigation of the effect of insoluble surfactants on drop deformation and breakup in simple shear flow. *J. Colloid Interface Sci*. **298**, 369–394.

Brenner, M. P., Shi, X. D. & Nagel, S. R. 1994 Iterated instabilities during droplet fission. *Phys. Rev. Lett*. **73**, 3391–3394.

Chandrasekhar, S. 1961 *Hydrodynamic and Hydromagnetic Stability*. Oxford University Press.

Chauhan, A., Maldarelli, C., Rumschitzki, D. & Papageorgiou, D. 2003 An experimental investigation of the convective instability in a jet. *Chem. Engng Sci*. **58**, 2421–2432.

Chen, A. U., Notz, P. K. & Basaran, O. A. 2002 Computational and experimental analysis of pinch-off and scaling. *Phys. Rev. Lett*. **88**, 174501.

Craster, R. V. & Matar, O. K. 2007 On autophobing in surfactant-driven thin films. *Langmuir* **23**, 2588–2601.

Craster, R. V., Matar, O. K. & Papageorgiou, D. T. 2002 Pinchoff and satellite formation in surfactant covered viscous threads. *Phys. Fluids* **14**, 1364.

Craster, R. V., Matar, O. K. & Papageorgiou, D. T. 2005 On compound threads with large viscosity contrasts. *J. Fluid Mech*. **533**, 95–124.

Denn, M. M. 1980 Drawing of liquids to form fibers. *Annu. Rev. Fluid Mech*. **12**, 365–387.

Edmonstone, B. D., Craster, R. V. & Matar, O. K. 2006 Surfactant-induced fingering phenomena beyond the critical micelle concentration. *J. Fluid Mech*. **564**, 105–138.

Eggers, J. 1993 Universal pinching of 3D axisymmetric free-surface flow. *Phys. Rev. Lett*. **71**, 3458–3460.

Eggers, J. 1995 Theory of drop formation. *Phys. Fluids* **7**, 941–953.

Eggers, J. 1997 Nonlinear dynamics and rupture of breakup of free-surface flows. *Rev. Mod. Phys*. **69**, 865–929.

Eggers, J. & Dupont, T. F. 1994 Drop formation in a one-dimensional approximation of the Navier–Stokes equation. *J. Fluid Mech*. **262**, 205–221.

Eggers, J. & Villermaux, E. 2008 Physics of liquid jets. *Rep. Prog. Phys*. **71**, 036601.

Eggleton, D., Pawar, Y. P. & Stebe, K. J. 1999 Insoluble surfactants on a drop in an extensional flow: A generalization of the stagnated surface limit to deforming interfaces. *J. Fluid Mech*. **385**, 79–99.

Eggleton, C. D. & Stebe, K. J. 1998 An adsorption desorption-controlled surfactant on a deforming droplet. *J. Colloid Interface Sci*. **208**, 68–80.

Gaver III, D. P. & Grotberg, J. B. 1992 Droplet spreading on a thin viscous film. *J. Fluid Mech*. **235**, 399–414.

Hameed, M., Siegel, M., Young, Y. N., Li, J., Booty, M. R. & Papageorgiou, D. T. 2008 Influence of insoluble surfactant on the deformation and breakup of a bubble or thread in a viscous fluid. *J. Fluid Mech*. **594**, 307–340.

Hansen, S., Peters, G. W. M. & Meijer, H. E. H. 1999 The effect of surfactant on the stability of a fluid filament embedded in a viscous fluid. *J. Fluid Mech*. **382**, 331–349.

Hunter, R. J. 1991. *Foundations of Colloid Science*. Oxford Science.

Jensen, O. E. & Grotberg, J. B. 1993 The spreading of heat or soluble surfactant along a thin film. *Phys. Fluids* A **5**, 58–68.

Jin, F., Gupta, N. R. & Stebe, K. J. 2006 The detachment of a viscous drop in a viscous solution in the presence of a soluble surfactant. *Phys. Fluids* **18**, 022103.

Keast, P. & Muir, P. H. 1991 Algorithm 688 EPDCOL – a more efficient PDECOL code. *ACM Trans. Math. Software* **17**, 153–166.

Keller, J. B., Rubinow, S. L. & Tu, Y. O. 1973 Spatial instability of a jet. *Phys. Fluids* **16**, 2052.

Kwak, S. & Pozrikidis, C. 2001 Effect of surfactants on the instability of a liquid thread or annular layer. Part I. Quiescent fluids. *Intl J. Multiphase Flow* **27**, 1–37.

Lee, H. C. 1974 Drop formation in a liquid jet. *IBM J. Res. Dev.* **18**, 364–369.

Leib, S. J. & Goldstein, M. E. 1986*a* Convective and absolute instability of a viscous jet. *Phys. Fluids* **29**, 952.

Leib, S. J. & Goldstein, M. E. 1986*b* The generation of capillary instabilities on a liquid jet. *J. Fluid Mech.* **168**, 479.

Liao, Y.-C., Franses, E. I. & Basaran, O. A. 2006 Deformation and breakup of a stretching liquid bridge covered with an insoluble surfactant monolayer. *Phys. Fluids* **18**, 022101.

Liao, Y.-C., Subramani, H. J., Franses, E. I. & Basaran, O. A. 2004 Effects of soluble surfactants on the deformation and breakup of stretching liquid bridges. *Langmuir* **20**, 9926–9930.

Lin, S. P. & Reitz, R. 1998 Drop and spray formation from a liquid jet. *Annu. Rev. Fluid Mech.* **30**, 85–105.

Link, D. R., Anna, S. L., Weitz, D. A. & Stone, H. A. 2004 Geometrically mediated breakup of drops in microfluidic devices. *Phys. Rev. Lett.* **92**, 054503.

McGough, P. T. & Basaran, O. A. 2006 Repeated formation of fluid threads in breakup of a surfactant-covered jet. *Phys. Rev. Lett.* **96**, 054502.

McKinley, G. H. & Tripathi, A. 2000 How to extract the Newtonian viscosity from capillary breakup measurements in a filament rheometer. *J. Rheol.* **44**, 653–670.

Notz, P. K., Chen, A. U. & Basaran, O. A. 2001 Satellite drops: unexpected dynamics and change of scaling during pinch-off. *Phys. Fluids* **13**, 549–552.

Papageorgiou, D. T. 1995*a* Analytical description of the breakup of liquid jets. *J. Fluid Mech.* **301**, 109–132.

Papageorgiou, D. T. 1995*b* On the breakup of viscous liquid threads. *Phys. Fluids* **7**, 1529–1544.

Rayleigh, L. 1878 On the stability of liquid jets. *Proc. London Math. Soc.* **10**, 4–13.

Rothert, A., Richter, R. & Rehberg, I. 2003 Formation of a drop: viscosity dependence of three flow regimes. *New J. Phys.* **5**, 59.

Schulkes, R. M. S. M. 1993 Dynamics of liquid jets revisited. *J. Fluid Mech.* **250**, 635–650.

Shi, X. D., Brenner, M. P. & Nagel, S. R. 1994 A cascade of structure in a drop falling from a faucet. *Science* **265**, 219–222.

Song, Q., Couzis, A., Somasundaran, P. & Maldarelli, C. 2006 A transport model for the adsorption of surfactant from micelle solutions onto a clean air/water interface in the limit of rapid aggregate disassembly relative to diffusion and supporting dynamic tension experiments. *Colloids Surf.* A **282–283**, 162–182.

Stebe, K. J. & Maldarelli, C. 1994 Remobilizing surfactant retarded fluid particle interfaces. 2. Controlling the surface mobility at interfaces of solutions containing surface-active components. *J. Colloid Intl Science* **163**, 177–189.

Timmermans, M.-L. E. & Lister, J. R. 2002 The effect of surfactant on the stability of a liquid thread. *J. Fluid Mech.* **459**, 289–306.

Tomotika, M. 1935 On the instability of a cylindrical thread of a viscous liquid surrounded by another viscous liquid. *Proc. R. Soc. Lond.* A **150**, 322–337.

Wang, J., Mohebi, M. M. & Evans, J. R. G. 2005 Two methods to generate multiple compositions in combinatorial ink-jet printing of ceramics. *Macromol. Rapid Commun.* **26**, 304–309.

Wang, Y., Papageorgiou, D. T. & Maldarelli, C. 1999 Increased mobility of a surfactant-retarded bubble at high bulk concentrations. *J. Fluid Mech.* **390**, 251–270.

Wang, Y., Papageorgiou, D. T. & Maldarelli, C. 2002 Using surfactants to control the size of wakes behind moving bubbles at order one Reynolds numbers. *J. Fluid Mech.* **453**, 1–19.

Wilkes, E. D., Phillips, S. D. & Basaran, O. A. 1999 Computational and experimental analysis of dynamics of drop formation. *Phys. Fluids* **11**, 3577–3598.

Zhang, X. & Basaran, O. A. 1995 An experimental study of dynamics of drop formation. *Phys. Fluids,* 1184–1203.

Zhang, X., Harris, M. T. & Basaran, O. A. 1994 Measurement of dynamic surface tension by a growing drop technique. *J. Colloid Interface Sci.* **168**, 47–60.